A MULTIDISCIPLINARY STRATEGY FOR THE INSPECTION OF HISTORICAL METALLIC TIE-RODS: THE MILAN CATHEDRAL CASE STUDY

Bellanova Mariagrazia[1]

Felicetti Roberto[1]

[1] Department of Civil and Environmental Engineering, Politecnico di Milano, piazza Leonardo da Vinci, 32, 20133, Milano, Tel: +39 02 23994388 - Fax: +39 02 23994220 mariagrazia.bellanova@polimi.it, roberto.felicetti@polimi.it

Corresponding author: Bellanova Mariagrazia

Abstract

A reliable assessment of historical metallic tie-rods requires both the estimation of actual tensile load and the identification of dominant defects. Despite of high defectiveness resulting from traditional metalworking techniques, so far the latter aspect has not been duly addressed in the literature. In this paper, several methodologies are discussed aimed at integrating the usual inspection practice. All studies were performed on the tie-rods of Milan Cathedral. Metallurgical analyses allowed to recognize the main features of the material. Mechanical characterization in the perspective of Elasto-Plastic Fracture Mechanics (EPFM) indicated the conditions for crack propagation. Several Non-Destructive Techniques (NDTs) commonly used in Mechanical Engineering (i.e. guided waves, eddy currents, pulsed active thermography) were examined and adapted to this unconventional application. Based on the combination of all the mentioned methods, a multidisciplinary procedure was defined, which allows the evaluation of the crack significance with reference to the estimated working stress.

Keywords: tie-rods, wrought iron, toughness, non-destructive testing, Milan cathedral

1. Introduction

Since the 14th century, metallic tie-rods have been extensively used in historical buildings to reduce the horizontal thrusts induced by vaults and to prevent the vertical walls overturning (Mastrodicasa 1974). Therefore, the assessment of their mechanical behaviour is a decisive step for the structural safety evaluation of the whole building. Research on this topic is currently focused on the estimation of the actual tensile stress of the tie-rods. Many methods have been developed, which are usually based on the correlation between the tension state and the dynamic response of the element (Lagomarsino and Calderini 2005). Despite such evaluation is essential, in most cases the mentioned approaches do not take into account the presence of dominant defects, which may strongly influence the bearing capacity of historical metallic ties. Indeed these latter were manufactured according to traditional metalworking processes and hence high defectiveness at different scales occurs (Percy 1864). Ancient furnaces were usually characterized by a low reducing power and thermal conditions were not uniform. As a consequence, very heterogeneous metal matrixes resulted with many non-metallic slag inclusions at the microscale, local porosities, and larger voids (Tylecote 1999, Nicodemi 2004). Moreover, macro discontinuities and rough surface can be recognized due to manual forging. The typical macro-defects of tie-rods are the so-called “bolliture”, namely forged welds used to joint several wrought iron bars in order to manufacture a longer workpiece (Musso and Copperi 1877). Therefore, localization and characterization of defects, as well as evaluation of their effects on the global behaviour of the inspected element, cannot be disregarded while examining historical metallic tie-rods. Based on these premises, several correlated researches were conducted with the aim of defining a multidisciplinary and multiscale assessing procedure, able to account for the presence of defects and hence to achieve more reliable results (Bellanova, 2017). In order to fulfil this purpose, two main topics were tackled: material characterization and non-destructive diagnosis. Despite both of them are commonly addressed

in the field of cultural heritage, they have not been thoroughly studied with reference to historical metallic tie-rods and are still open issues.

2. Case study

The studies discussed in this paper were carried out on tie-rods of Milan cathedral, which show very interesting and peculiar features. Compared to the same kind of structural elements in other historical buildings, they exhibit a remarkably larger cross-sections (average dimensions about 55x85 mm^2). Their length and height from the floor depend on the considered nave and varies from 5.10 m to 16.4 m and from 16.5 m to 34.2 m, respectively (Figure 1). Usually, tie-rods were used as temporary elements during construction or as added braces (Mastrodicasa 1974). Contrary to this practice, in Milan cathedral they were included in the original structural system. A document dating back to 1400 concerning the response of Duomo's engineers to Minot's doubts on the quality of the project testifies the intention to use these elements from the beginning of the construction (Veneranda Fabbrica del Duomo 1877). Therefore, most of them have been in service for more than five centuries. Moreover, tie-rods have an even more important role in Milan cathedral compared to in other coeval churches (Heyman 1995), due to the unusual structural system of the building resulting from the contamination between European gothic style and Lombard tradition (Ferrari da Passano 1988). Indeed the buttresses have small dimensions and hence their contribution is limited. The flying buttresses were added in the 19th century, above the points where the lateral thrusts act. The spires were built in the 18th century and hence their effect is recent. For these reasons, horizontal thrusts are mainly balanced by the tie-rods and the walls located above the transversal gothic arches of the lateral naves. Over the centuries, the permanent loads have remarkably changed due to the completion of the cathedral. The most critical phase was the controversial erection of the tiburio (15th century). It led to severe structural damages and the construction was stopped for more than 20 years (Coronelli, Caggioni, and Zanella 2015).

Furthermore, load paths were modified due to other significant occurrences. Among them, in the 20th century, the water draining by industrial companies caused a groundwater level lowering by about 25 m in the area around the cathedral and, consequently, severe subsidence phenomena and differential settlements occurred (Coronelli et al. 2014). This exacerbated the conditions of the structures leading to restoration in the 20th century, which was carried out by a team from Politecnico di Milano and Istituto Sperimentale Modelli E Strutture (ISMES), under the supervision of the Veneranda Fabbrica del Duomo in the person of Carlo Ferrari da Passano (Ferrari da Passano 1980, Ferrari da Passano 1988).

In May 2009 the deformation monitoring system working inside the cathedral recorded an anomalous verticality variation of a pillar compared with the previous years trend (Giussani 2015). Examination of the involved area revealed a tie-rod failure (indicated as T01 in Figure 1) and the ancient wrought iron bar was substituted with a modern steel one. Few years later, during visual inspection a very deep crack was identified in another tie-rod (indicated as T02 in Figure 1), which was replaced in 2013. After these events, a wide multidisciplinary study on tie-rods of Milan cathedral was launched to evaluate their state of conservation and the two failed elements were made available to Politecnico di Milano for the experimental investigation. More precisely T01 was used to machine samples for the material characterization performed in this work as well as in a former study (M. Vasic 2015). On the contrary, T02 was preserved and used as a benchmark to calibrate NTDs discussed in this assay.

Preliminary tensile tests were carried out according to the standard EN ISO 6892-1 on eight samples machined from T01 (M. Vasic 2015). Results showed a very high standard deviation. In particular, yield stress, tensile strength, and elastic modulus were found to be equal to 142 ± 60 MPa, 199±111 MPa and 206 ± 45 GPa, respectively. Finally, the density was measured using the hydrostatic weighing method and resulted to be equal to 7792 kg/m^3. On site investigation by implementing the dynamic identification method proposed by (Tullini and

Laudiero 2008) allowed the estimation of the actual state of stress of 112 tie-rods (M. Vasic 2015). The experimental campaign provided very interesting results, showing stress values in the range 0 - 150 N/mm^2.

However, a careful detection of dominant defects was still required in order to assess the safety of the most stressed elements. In this framework, the studies discussed in this paper were developed.

3. Material characterization

In the past no theoretical knowledge on metal manufacturing processes was available. The artisans learned to produce artefacts in the workshops in accordance with the best practice. The quality of the products strongly depended on the master's ability and it was not repeatable. Therefore, metallurgical characterization is needed to study the main features of the material which may influence the mechanical behaviour of the final object as well as the applicability of the Non-Destructive Testing (NDTs). In (Vecchiattini, Calderini, and Piccardo 2015) a metallurgical investigation on many Italian tie-rods samples was performed with the aim of establishing possible recurring features. As discussed in (Dillman and L'Héritier 2007) the study of slag inclusions may provide useful insights for characterizing ferrous alloys. Moreover, interesting information can be achieved by studying the failure of the two removed tie-rods to recognize any possible recurring aspect. In order to achieve these objectives, the breaking surface of the tie-rod T01 and a cut section close to it were examined by using many combined techniques, i.e. Stereoscopic Microscopy (SM), Light Optical Microscopy (LOM), Scanning Electron Microscopy (SEM), Energy Dispersive X-ray Spectroscopy (EDXS), Vickers (HV) and Rockwell (HR) hardness tests. The average dimensions of T01 were about 55x80mm^2, while its length is about 6.8 m.

Metallurgical characterization highlighted significant inherent material defectiveness. Additionally, macroscopic forged welds are expectable considering tie-rods dimensions. For

these reasons, toughness turned out to be a more significant parameter to characterize the mechanical properties of the material. Preliminary tests based on Linear Elastic Fracture Mechanics (LEFM) proved to be not reliable, due to the remarkable ductility of the material. Further tests in the framework of Elasto Plastic Fracture Mechanics (EPFM) were implemented in order to account for plasticity (Anderson 1994). Single Edge-Notched Bend (SEB) specimens were machined from T01, according to the prescriptions reported in the standard ASTM E1820, i.e. 130 x 25.4 x 12.7 mm. The effects of forged weld on mechanical behaviour were considered. Seven samples of base material and six samples including a welded joint at notch were tested in total.

An overview on the localization of samples used for material characterization is summarized in Figure 2.

3.1 Microstructure

The fracture surfaces of the failed tie-rod were thoroughly studied by SEM. Since results are completely repeatable, in this paper only those pertaining to one of them (sample A, Figure 2) are shown. Typical images are displayed in Figure 3. In the picture at lowest magnification (Figure 3b), areas with different features can be recognized. Figure 3c reveals a transgranular brittle failure through a clear identification of both cleavage planes and river patterns. Figure 3d clearly shows dimples, indicating micro void coalescence around an inclusion. The latter has a silicates-rich chemical composition, as highlighted by EDXS analysis. This observation suggests a low reducing iron-smelting atmosphere. Often brittle and ductile failure modes were identified very close one to each other all over the fracture surfaces, indicating a heterogeneous microstructure.

A cross-section close to the fracture surface (sample B, Figure 2) was inspected by LOM in order to characterize the material at the microscale (ASTM E 3-11). A micrograph at 100X was taken at each node of a 40-points grid (10 mm spacing). In each picture, the fractions of

microstructural compounds were determined according to ASTM E 562-02. The discrete data system was transformed into a continuous distribution by interpolating the nodal values. Ferrite and pearlite are the most recurring microstructures but their percentage over the cross-section is extremely variable as can be observed in Figure 4. Two distinct more homogenous areas can be identified. At the interface between them, the amount of the two microstructural compounds is comparable. Only along this latter line, grains exhibit large and different dimensions. Often Widmanstätten plates can be observed, suggesting a direct production process (Ashkenazi et al. 2012). Mostly ferritic structure is prevalent and characterizes the 78% of the examined grid nodes. Increasing the percentage of pearlite, the amount of carbon raises and hence also strength and brittleness.

Very interesting features were detected by LOM on the fractured area across the crack. Before etching, concentrated discontinuities were locally identified (Figure 5a). After etching, sudden change of both microstructure and grains size was highlighted as well. As can be seen in Figure 5b, the crack seems to be propagated at the boundary between these two patterns. In the literature, these features are often associated to a forged weld between two pieces characterized by dissimilar compositions (L' Hèritier et al. 2013, Menzemer et al. 2016).

Many types of defects were recognized by using SM, such as micro-cracks, micro-porosities, voids, slag inclusions. SEM coupled with EDXS allowed their characterization. A strong correlation was found between metal matrix and type of discontinuities. Iron-rich dendritic slag inclusions (typically wüstite) characterize the mostly ferritic matrix (Figure 6a). Spheroidal graphitic carbon is often identified as well. Fine pearlite nucleates around carbon nodules (Figure 6b). These features cannot be recognized in the mostly pearlitic microstructure, where smaller glassy slag (Figure 6c) and microcracks were detected. Crack propagated toward the mostly pearlitic structure. Usually iron oxides inclusions are located inside the crack (Figure 6d).

Vickers and Rockwell hardness tests were performed as well at the same location of LOM analyses by shifting the two measurements by 4mm in order to avoid any interaction. In Figure 7 the two corresponding contour plots are compared. Large standard deviations (55 HV10 and 9.2 HR) confirm the heterogeneity detected by the previous inspections. The Vickers data fall in the interval of 79 - 284 HV10 and have a mean value of 132 HV10. The Rockwell values span over a maximum of 79 HR and a minimum of 50 HR and have a mean value of 61 HR. The results show a good agreement with the microstructural findings: higher hardness values correspond to mostly pearlitic microstructure, while the lowest ones to mostly ferritic microstructure. Further details on the material characterization of tie-rods of Milan cathedral can be found in (Bellanova et al. 2015).

3.2 Fracture properties

Elasto Plastic crack initiation testing was performed according to ASTM E1820-17. It is based on the acquisition of the load-displacement curve including loading-unloading cycles at defined crack length increments. From this curve, the J-R plot is achieved by computing the J-integral value at the corresponding crack length increment through the contribution of its elastic and plastic components. Thus, the critical J-integral value can be determined.

In Figure 8 and Figure 9 the obtained load-displacement curves and J-R curves are shown, by overlapping on the same plot the typical results from a sample of base material (blue curve) and a sample including a forged weld (red curve). A very different mechanical behaviour is observed. As can be seen in Figure 8, during crack propagation, the energy dissipated by the sample of base material is remarkably higher and hence a greater toughness value is expected. A hardening branch dominates the load-displacement curve: after the linear-elastic portion, strong deformations correspond to relatively small load increments. Plastic deformation is very high and the ultimate strength is never reached. No-local instabilities are recognized. J integral values at each loading/unloading point are very spread and they cannot be properly interpolated

as described in ASTM E1820-17. Therefore, J_{IC} cannot be qualified by using the mentioned standard. The highest measured J-value can be assumed as a rough estimate of J_{IC}.

On the contrary, the load-displacement curve of the sample including the forged-weld is characterized by a softening branch: after the ultimate strength, deformation increments correspond to load decrements. Sometimes unstable crack propagations can be recognized which could be associated to the presence of local discontinuities. As it is shown in J-R curve in Figure 9, the distribution of J integral values at each loading/unloading cycle is more regular and the J_{IC} parameter can be estimated in almost all specimens.

The observation of specimens after testing clearly confirms the experimental data. Samples including forged weld are nearly broken in two parts and crack propagation pattern is not straight but follows an inclined path, probably corresponding to the welding line (Figure 10a). On the contrary, in samples machined from base material crack propagated through a very limited portion of the thickness (Figure 10b).

Due to the high material heterogeneity, the J_{IC} values computed for all examined samples are rather spread. However, the two classes can be clearly recognized. The average value of the estimated parameter in the base material is one order of magnitude higher (approximately 330 MPa mm) than in the jointing interface (approximately 40 MPa mm). Despite these values cannot represent the quality of the whole element, they provide very interesting information on the mechanical properties of material and led to the conclusion that the regions including forged welds are the most critical cross-sections of the tie-rods.

Acoustic emission monitored during EPFM testing confirmed these results, as discussed in (Gianneo et al. 2017).

4. Non-destructive crack survey

Nowadays, no methods specifically designed for dominant crack detection in historical tie-rods are available. Many established Non-Destructive Techniques (NDT) are commonly used

to detect cracks in modern metallic components but heterogeneity, roughness, and defectiveness might compromise their effectiveness on ancient metals (IAEA, International Atomic Energy Agency 2011). Therefore several NDTs were studied in order to figure out if and how their application could be extended to the field of cultural heritage. A multiscale approach was chosen because it ensures a remarkable reduction of time and costs. Three levels of inspection were recognized: global, intermediate, and local. The Guided Waves method (GW) turned out to be a very promising technique at the global scale, whose aim is a quick discrimination between damaged and undamaged elements. Guided waves are high frequency vibrations propagating through elongated structures. Due to the guiding effect of the boundaries, they can propagate for long distances with a little loss of energy, allowing the inspection of the whole elements by performing just a few measurements (Zhongqing and Lin 2009). Once damaged tie-rods are recognized, defective regions are localized at the intermediate scale. After preliminary evaluations, Eddy current Testing (ET) was chosen to this purpose because it is an electromagnetic method not requiring the use of couplant and then suited for scanning long elements. Another great advantage of ET is the possibility to easily build special probes matching the test requirements. The method is based on the induction of eddy currents in conductive materials by way of alternated magnetic field produced by a coil. Any discontinuity disrupts these currents and is revealed as a change of impedance of the coil (Blitz 1991). At the local scale, flaw characterization is carried out. In this work the Pulsed active Thermography (PT) was studied (Maldague 2001) by way of both experimental and numerical approaches in order to evaluate its capability to estimate crack size and position.

4.1 Guided waves method

Despite the use of guided waves for the inspection of historical tie-rods shows very interesting features, the implementation of the method is made difficult by their complex way

of propagation. In fact, many modes are excited simultaneously whose propagation velocity is not constant but depends on frequency and element thickness. During the travelling through the medium, the diagnostic pulse is distorted, since its frequency components propagate at different velocity (dispersive waves). For these reasons, the effectiveness of the method depends on the accurate setting of operational parameters based on a detailed study of propagation modes (Zhongqing and Lin 2009).

Experimental laboratory analyses were performed on the original tie-rod T02 of Milan cathedral that was replaced due to the presence of a deep crack. Data acquisition was performed by using the A1040 MIRA ultrasonic low frequency tomograph (by Acoustic Control System, Russia) exploiting the great advantage of its sensor array made of 12 blocks of 4 Dry Point Contact (DPC) transducers loaded by independent springs (Bellanova et al. 2017). This device allows to overcome the problem of surface roughness, thanks to the quick dry coupling between the probes and the sample. In a few seconds, the device emits and receives ultrasonic shear pulses between any combination of emitter and receiver blocks (66 waveforms in total). The signal processing was performed by implementing the focusing procedure described in (Wooh and Shi 2001), properly modified to account for the specific features of the used device. As outlined in Figure 11 the collected signals are shifted along the time axis in order to offset the different probes distance to any reflector. Then they are combined into a synthetic wave, which is cross-correlated with the original diagnostic wave in order to reduce the noise effects and enhance the sharpness of indications.

Dispersion curves were computed to identify the properties of a least dispersive diagnostic wave. The analytical polynomial approach described in (Yu et al. 2015) was implemented to this purpose by assuming a rectangular cross-section with dimensions comparable to the tie-rods of Milan cathedral. The results are shown in Figure 12a. The colored curves indicate modes that may be detected by the device based on the array configuration and the sensitivity

to just shear vibrations on the test surface. As can be observed, the most appropriate frequency range is 10-20 kHz, where just two not very dispersive modes are involved. Unfortunately this test configuration cannot be implemented due to the restrictions imposed by the technical features of the device. For this reason, a diagnostic wave characterized by a central frequency of 25 kHz and a pulse length of 2 cycles was used. By overlapping the corresponding spectrum (Figure 12b) with the dispersion curves, it can be observed that many dispersive modes are excited simultaneously.

Nevertheless, the effectiveness of the method was evaluated by performing measurements at a known distance (i.e. 1.2 m) from the macroscopic defect of T02, which is a deep crack characterized by a maximum opening of about 1.5 mm. The achieved amplitude-distance plot is shown in Figure 13. A peak can be easily recognized at the distance corresponding to crack location and noise is fairly low (about the 5% of the peak amplitude). Despite of the not optimal test configuration, the results are promising.

4.2 Eddy current testing

Every discontinuity of geometry (roughness, shape, dimensions) and material (density, non-metallic inclusions, void, microstructure, etc.) may alter eddy currents path, increasing the probability false indications (García-Martín, Gómez-Gil, and Vázquez-Sánchez 2011). Based on these premises and considering the remarkable heterogeneity of wrought iron, eddy current testing has to be optimized in order to sense just dominant defects, while neglecting insignificant variations. In tie-rods, cracks may initiate inside the cross section and hence a higher penetration depth is required. The execution time has to be taken into account as well.

Several parameters can be considered for measuring the electrical variations due to discontinuities. Impedance is the most commonly used one and it was adopted for the investigations discussed in this paper. An off-the-shelf low frequency spot probe (Olympus U8626005) was used for a preliminary assessment of the eddy currents effectiveness in

detecting dominant cracks in the tie-rods at issue. A penetration depth of about 15 mm was estimated experimentally (without considering the effect of the surface oxidation layer). The tie-rod T02 was inspected by scanning all its four sides. The achieved indications survey is shown in Figure 14. The results do not completely fulfill the test requirements because many indications were detected and the dominant defects cannot be recognized unambiguously. However in four regions, indicated as Critical Section (CS) in Figure 14, the recorded indications showed very interesting features: sharp and strong variation of impedance were identified along the whole width of at least three tie-rod sides. One of them is the region with the macroscopic crack leading to the tie-rod replacement. In order to validate the results of eddy current testing, Magnetic Particles Inspection (MPI) was carried out according to ISO 3059. It revealed at each CS position a continuous discontinuity over the whole perimeter having the typical forged weld shape, i.e. inclined at about 27° on the smaller sides and rather rounded on the larger ones (Figure 15).

Based on these results, a more performant probe prototype was built, which was devised to localize just these most critical regions. The horseshoe typology was chosen because it provides a very large field of action, allowing the inspection of the whole depth of a tie-rod side in just one take. Consequently a strong reduction of the spatial resolution arises which implies neglecting the secondary defects and hence fulfilling test requirements. For the same reason, geometry, shape, and number of turns were optimized to inspect the whole cross-section and a low operative frequency (i.e. 500 Hz) was adopted. The horseshoe probe is made of two coils wound on a U-shaped ferromagnetic core, inducing eddy currents rather orthogonal to the orientation of the discontinuity. Thus, a stronger perturbation of eddy currents path results and hence the signal amplitude is more intense. Interchangeable polyethylene caps were used to protect the poles from wear against the uneven and rough tie-rod surface. Clear peaks characterized by strong amplitude were recognized only at CS locations. Noise was very low

and did not affect the results. Based on these evidences, it can be concluded that the customized probe is a viable tool for on-site inspection. A more complete test description is provided in (Bellanova et al. 2017).

4.3 Active thermography

In traditional active thermography, indications are achieved from a single thermogram, representing the temperatures distribution at a given time. According to this approach, prolonged heating is generally needed to involve the whole element thickness. In case of the metallic tie-rods, high conductivity of the material prevents from obtaining a sufficient temperature contrast over the inspected surface. Furthermore, roughness, rust and localized material heterogeneities imply different local values of emissivity over the surface. In order to overcome these drawbacks, the Pulsed Thermography (PT) method was used and the time evolution of the thermal pictures was considered (Maldague, Galmiche, and Ziadi 2002). In-transmission method of observation allowed the inspection of the whole tie-rod thickness.

Bi-dimensional numerical simulations were performed to evaluate the effects of crack geometry, length, and position as well as the incidence of diffusion toward unheated regions. A step heating of +10° C lasting 20 seconds was used to simulate the thermal pulse. Different crack lengths were modelled. Emerging and non-emerging conditions were considered as well. Figure 16 shows the numerical simulation results in terms of the evolution of the temperature variation along a central strip. Every configurations showed the maximum contrast between defective and no-defective region after about 60 seconds. In the plots pertaining to the emerging crack (Figure 16 b, d and f) the sharp discontinuity indicates the crack tip. Defective regions can be distinguished unambiguously from the non-defective ones. One region characterized by high thermal gradients can be recognized. Its length is proportional to the crack size and it is approximately one-and half times the crack length. In the plots representing the non-emerging crack conditions (Figure 16 c and f) the variation of temperature is smoother. In the first stages

of the simulation, the main peak is placed in the middle of the crack projection, but it moves towards the crack mouth, placed on the opposite side.

Numerical analyses were validated by performing experimental tests on the tie-rod T02 characterized by the visible crack. Along this element, four different conditions can be recognized after magnetic particle inspection: region without discontinuity, emerging macroscopic crack at forged weld, non-emerging macroscopic crack at forged weld, minor emerging crack at forged weld detected by eddy current testing. With the objective of avoiding the heat losses through the upper and lower sides of the tie-rod and to promote a planar heat flow, the setup shown in Figure 17 was arranged. The distributions of the maximum temperature reached at each point on the unexposed surface and of the corresponding time were used as indicators for the time analysis of thermograms. The plots pertaining to the region characterized by the macroscopic crack are shown in Figure 18 and Figure 19. As can be observed, the results are very effective both in emerging and non-emerging conditions. However, in the other examined regions, the same representation does not provide equally compelling outcomes. Clearer indications were obtained by plotting the evolution of the temperature variation along a central strip, as shown in Figure 20. Despite of the noise effects, the experimental results are in full agreement with the numerical analyses. A sharp discontinuity can be recognized in the plots corresponding to the emerging cracks. A stronger perturbation is associated to the macroscopic emerging crack (Figure 20b) whereas the isotherms slope at the welding joint including a minor crack is smaller (Figure 20c). On the contrary, a smoother variation is identified by taking thermal pictures over the surface where the crack does not emerge (Figure 20d).

In summary, though many improvements are required to regard pulsed active thermography as a reliable tool to characterize cracks, at this phase of the research it allows to distinguish emerging from non-emerging defects. In this latter case, information on crack extension can be

inferred as well. The studies performed on the application of active thermography for crack detection in historical tie-rods are reported in detail in (Bellanova 2017)

5. Proposed procedure and in situ inspection

In any historic metallic component, the presence of defects is unavoidable. Therefore, it is important to understand the significance of the detected flaws in connection with the actual loading conditions. The performed research, combined with other established methods, allowed to define guidelines to perform a complete assessment of the structural safety of the historical metallic tie-rods, accounting for the presence of dominant defects. The flow chart of the proposed procedure is shown in Figure 21.

Due to the inherent material heterogeneity and the presence of weaker sections (i.e. forged welds), fracture mechanic turned out to be the most consistent approach to examine these regions. Consequently the variables involved in the evaluation of crack significance are fracture toughness, actual sustained load, and flaw size. The latter parameter can be estimated by performing the multilevel diagnostic inspection addressed in this work. At the global and intermediate scales, very interesting results were obtained by using the guided waves method and eddy current testing respectively. As discussed before, these techniques have to be customized for this unconventional application. At the local inspection scale, active thermography allows the localization of significant flaws inside the defective regions, but only a rough estimation of the crack length can be achieved. More precise sizing requires further improvements. As an alternative, the ultrasonic phased array method could be used. Preliminary tests on the dismissed tie-rods proved the effectiveness of this established technique. However, being a time-demanding method because of the small tested volume, it can be viably used just in a few selected sections. Moreover, friction with the rough and abrasive tie-rod surface tends to wear and damage the sensitive part of the transducers array.

Fracture toughness was determined experimentally. The order of magnitude of this parameter was estimated despite of the rather spread results. Due to the reduced ductility, the value at forged weld has to be considered because it corresponds to the easiest crack propagation. For linear elastic cases, the obtained critical value of J-integral J_{IC} can be easily converted in the critical stress intensity factor K_{IC} according to the equation below:

$$J_{IC} = \mathcal{G}_{IC} = \frac{K_{IC}^2}{E'} \tag{1}$$

Where the $\mathcal{G}_{IC}$ is the critical energy release rate and E' is the elastic modulus.

As concerns the estimation of the actual sustained average stress of the tie-rods, many techniques have been proposed in the last 15 years (Tullini and Laudiero 2008).

The significance of the crack dimensions can be evaluated in terms of either critical crack size or critical state of stress. According to the first procedure, once the actual stress and the material toughness are known, the critical crack length dimension can be computed. Assuming a bi-dimensional problem, after the initiation, flaws may propagate along either an orthogonal or an inclined direction relative to the tie-rod axis. In the first case, pure mode I takes place and the following relationship can be used:

$$K_{IC} = \sigma_C Y_I \sqrt{\pi a} \tag{2}$$

where Y_I is the geometry factor in pure mode I, which is equal to 1.12 (VV. AA. 1987).

Otherwise, mixed mode I/II is involved and a reduction factor multiplying the critical stress intensity factor is introduced in order to account for the second mode:

$$K_{IC} \cdot \kappa = \sigma_C Y_I \sqrt{\pi a} \tag{3}$$

where κ is the ratio K_I/K_{IC} achieved by applying procedure described in (Chao and Liu 1997). By comparing the critical size a_c with the actual size a, two different conditions can be found: non critical crack ($a \ll a_C$) and uncertain condition ($a \approx a_C$). The latter case requires further

and accurate inspections to evaluate the tie-rod behavior in time because the tensile stress may change due to the seasonal temperature variations or the slow foundation settlements.

The first steps of the procedure were validated on site on seven tie-rods placed in the southern naves, close to tiburio, as highlighted in Figure 1. Historically this was one of the most suffering areas of the cathedral (Ferrari da Passano 1980) and nowadays it shows quite an interesting crack pattern on the vaults (Cardani, Coronelli, and Angjeliu 2016). The examined elements were chosen by comparing the results of the dynamic inspection (Vasic 2015), the displacement monitoring data recorded from the May 1988 to the November 2014 (Giussani 2015) and the corresponding trends of the mean strain. The tomograph MIRA A1040 was used to perform guided waves testing by collecting data on the larger vertical sides of the tie-rod. The recorded signals were processed by implementing the focusing procedure discussed before. Concerning eddy current testing, the probe prototype purposely built for this application was used. More emphasis was given to correlated indications characterized by two local strong variations of impedance, shifted by 100-200 mm on the opposite sides. Indeed these evidences are most likely due to the presence of an incipient crack along the forged weld. On the areas corresponding to eddy currents indications, a detailed visual inspection was performed as well. Pictures of 20 Mpixel resolution were taken by using Canon EOS 600 D high performance camera with an EF50mm f/2.5 compact macro lens, allowing close-up shooting up to 60 pixel/mm. Before taking pictures, the tie-rod surface was cleaned carefully.

Among the examined elements, the most critical condition was recognized on the tie-rod T04 Figure 1. On this element, eddy current testing allowed the identification of 14 indications, whose amplitude was either medium or strong (Figure 22a). Based on geometrical requirements, three couple of indications could be associated to forged welds. The most critical region is defined by indications In05 - In06. Indeed, in both cases the signal amplitude is rather high and a distance of about 120 mm separates the two peaks. The latter is exactly the length

between the two ends of a forged weld inclined about 27°. As can be observed in the high resolution pictures (Figure 22b), the eddy currents signals correspond to a continuous crack over three sides, with a maximum opening of 0.25 mm (15 pixels), which has never been identified before. The results of the guided waves in the same area are shown in Figure 23. Despite of the quite high noise amplitude (about the 25% of the maximum peak amplitude), a clear peak can be identified at location corresponding to crack. However, it is worth noting that crack detectability is strongly influenced by crack dimensions, due to a quite dispersive behaviour of the diagnostic wave allowed by the adopted device.

6. Concluding remarks

In this work the role of the dominant defects in the assessment of historical tie-rods is addressed. Two main topics were deeply studied: material characterization and non-destructive inspection.

Wrought iron was characterized by Stereoscopic Microscopy (SM), Light Optical Microscopy (LOM), Scanning Electronic Microscopy (SEM) and Energy Dispersive X-Ray Spectroscopy (EDXS) in order to identify the main features affecting mechanical behaviour. The material is remarkably heterogeneous in terms of both microstructure and incidence of defects. Ferrite and pearlite are the prevalent microstructural compounds but their distribution over the cross-section is extremely variable. Most of the examined cross-section (i.e. the 78% of the grid nodes) is characterized by a predominantly ferritic structure. As the percentage of pearlite increases, the amount of carbon raises and hence also strength and brittleness. In fact, the ferritic microstructure corresponds to the region of the failure surface exhibiting a more ductile failure mode, while the pearlitic microstructure was recognized mainly where transgranular brittle failure was identified. A good agreement between the hardness tests results and the microstructural findings was found: higher hardness values correspond to the pearlitic microstructure, while the lower ones are associated to the ferritic microstructure. A strong

correlation between the identified microstructures (ferrite, pearlite) and the type of discontinuities exists as well. Carbon-rich inclusions can be found in mostly pearlitic matrix while iron-rich inclusions characterize the ferritic matrix.

The failure of the two removed tie-rods was widely investigated at different levels. Crack leading to the failure of the tie-rod found broken in two portions probably initiated inside the cross section at a weaker point and propagated outward, along a forged weld. Moreover, Light Optical Microscopy (LOM) across visible crack revealed concentrations of inclusions and sudden variations of microstructure. In literature, these features are usually associated to forged welding. The macroscopic crack in the other substituted tie-rod propagated along a forged weld as well. Indeed, it exhibits the typical straight-scarf weld shape. Based on these evidences, it is reasonable to assume that forged welds are the weakest part of the elements at issue. This hypothesis was confirmed by Elasto Plastic Fracture Mechanics (EPFM) testing, revealing a J-integral value of wrought iron including a forged-weld one order of magnitude lower than base material. This parameter can be assumed as reference value to assess defect stability as a function of its size and sustained load.

The results obtained from material characterization and failure assessment of the dismissed tie-rods have proved the need to account for the dominant defects in an effective structural safety evaluation of these historical metallic elements. However, no viable techniques are nowadays available for their detection. For this reason, Guided Wave method (GW), Eddy current Testing (ET) and Pulsed active Thermography (PT) were studied to understand how they can be adapted to perform inspections at global, intermediate, and local scale respectively. Numerical and experimental approaches were used to recognize the limitations of each technique with respect to this unconventional application and how they can be overcome. At this stage of the project, the study on each method has reached different levels of progress,

especially concerning sensitivity to crack size, the adaption to different case studies and the ease of on-site implementation. An explanatory comparison is given in Table 1.

Concerning GW, the ultrasonic tomograph with an array antenna allowing the recording of 66 waveforms in few seconds was used to collect data. The latter were analysed by implementing a suitable focusing procedure. Both laboratory and on site experimental testing demonstrated that the effectiveness of this method strongly depends on crack dimensions. Increasing crack size, the reflection amplitude intensifies and hence the signal-to-noise ratio improves making the indication of the defect easier to recognize. Although this procedure has shown promising results, significant improvements are possible.

Studies on ET gave excellent outcomes. After unsuccessful attempts by using several off-the-shelf coils, a probe prototype was purposely designed and built in order to optimize the spatial resolution and hence to selectively detect just the dominant defects, neglecting all impedance variations due to localized discontinuities. The use of this probe allowed clear and quick detection of significant indications, which correspond to forged weldings.

Pulsed active Thermography (PT) was taken into account with the objective of localizing flaws and estimating their depth. A good agreement was found between numerical and experimental results. The evolution of temperatures along a reference path reveals the defective areas. This method may provide rough information on position and size of the inspected flaw. Sudden variation of thermal gradient indicates area affected by a flaw. Sharp or smooth trend at the boundary between defective and non-defective area suggests emerging or non-emerging crack respectively. A precise estimation of crack dimensions requires the improvement of the data processing.

The combination of the discussed studies with other established methods allowed to define a multidisciplinary and multiscale procedure to account for the dominant defects in the assessment of the structural safety of historical metallic tie-rods. The first three steps of the

proposed procedure (namely guided waves methods, eddy current testing, and detailed visual inspection) were validated on site on seven tie-rods placed in the lateral naves, close to tiburio. Many discontinuities were detected and classified in three categories, depending on the need for further inspections. Among them, a crack with a maximum opening of about 0.25mm, macroscopic on three sides of tie-rods, was identified. Although many previous visual examinations were performed, this defect had never been identified before.

The discussed work allowed to propose some viable coordinated tools and a specific material characterization procedure to address the still open issues of the structural safety of the historical wrought iron tie-rods. All studies have been carried out on tie-rods of Duomo but the defined guidelines can be easily adapted to any similar component.

Acknowledgments

The authors are grateful to Veneranda Fabbrica del Duomo (Milan, Italy) for the financial support given to this research project and for making available the failed tie-rods for the experimental studies. The work here discussed results from the fruitful collaboration among several research groups at Politecnico di Milano, which are also acknowledged. Metallurgical characterization was performed in collaboration with professors Giuseppe Silva, Barbara Rivolta and MSc. Andrea Baggioli, Mechanical Engineering Department of Politecnico di Milano (Lecco). Fracture Mechanics testing was carried out by the Laboratory of the Mechanical Engineering Department at Politecnico di Milano (Milano) under the supervision of professor Michele Carboni. Finally, the authors wish to thank Simone van der Meer, who actively contributed to the study on the guided waves method in partial fulfilment of her MS degree requirements at TU Delft (Netherland) in collaboration with Politecnico di Milano.

References

Acoustic Control System, Russia. 2015. *Operation manual A1040 MIRA ultrasonic low frequency tomograph.*

Anderson, T. L. 1994. *Fracture Mechanics.* London: Second Edition. CRC Press.

Ashkenazi, D., E. Mentovich, D. Cvikel, O. Barkai, A. Aronson, and Y. Kahanov. 2012. Archaeometallurgical Investigation of Iron Artifacts from Shipwrecks – A Review. In *Archaeology, New Approaches in Theory and Techniques*, by AA. VV., 169-186. InTech.

ASTM E 562-02: Standard Test Method for Determining Volume Fraction by Systematic Manual Point Count.

ASTM E 1820-17: Standard test method for measurement of fracture toughness.

ASTM E 3-11: Standard guide for preparation of metallographic specimens.

Bellanova, M. 2017. A multidisciplinary and multiscale strategy for the assessment of the structural safety of historical metallic tie-rods. PhD diss., Politecnico di Milano,.

Bellanova, M., A. Baggioli, B. Rivolta, R. Felicetti, and A., Cornaggia. 2015. Metallurgical and mechanical characterization of the historical tie-rod of Duomo di Milano. *Scienza e beni culturali - Metalli in architettura. Conoscenza, Conservazione, Innovazione.* 23-34. Bressanone: Arcadia Ricerche.

Bellanova, M., M. Cucchi, R. Felicetti, and F. Lo Monte. 2017. Unconventional applications of A1040 MIRA tomograph. Paper presented at the Conferenza Nazionale sulle Prove non Distruttive Monitoraggio Diagnostica. Milano.

Bellanova, M., R. Felicetti, M. Carboni, and A. Gianneo. 2017. Eddy current non destructive testing of historical metallic tie-rods. Paper presented at the Arte17, 12th International Conference on non-destructive investigations and microanalysis for the diagnostics and conservation of cultural and environmental heritage (Art.17). Turin, November 22nd/24th.

Blitz, J. 1991. *Electrical and magnetic methods of Non-Destructive Testing.* Bristol: Adam Hilger.

Cardani, G., D. Coronelli, and G. Angjeliu. 2016. Damage observation and settlement mechanisms in the naves of the Cathedral of Milan. *Structural analysis of historical constructions: anamnesis, diagnosis, therapy, controls: proceedings of the 10th international conference on structural analysis of historical constructions.* Leuven, Belgium.

Chao, Y. J., and S. Liu. 1997. On the failure of cracks under mixed-mode loads. *International Journal of Fracture*, 87(3): 201–223.

Coronelli, D., B. Caggioni, and F. Zanella. 2015. The Cathedral of Milan: the structural history of the load bearing system. *International Journal of Architectural Heritage* 9(4): 510–528.

Coronelli, D., C. di Prisco, F. Pisanò, S., Ghezzi, S. Imposimato, and M. Pesconi. 2014. The tiburio of the cathedral of Milan: structural analysis of the construction & 20th century foundation settlements. *Proceedings of the 15th International Conference on Structural Faults and Repair*. London, UK.

Dillman, P., and M. L'Héritier. 2007. Slag inclusion analysis for studying ferrous alloys employed in French medieval buildings: supply of materials and diffusion of smelting processes. *Journal of Archaeological Science* 34(11): 1810-1823.

Ferrari da Passano, C. 1988. *Il Duomo rinato [Milan cathedral reborn]*. Vigevano: Diakronia.

Ferrari da Passano, C. 1980. Interventi di consolidamento delle strutture del Duomo di Milano a seguito di fenomeni di subsidenza [Reinforcement interventions of the Milan Cathedral structures after the subsidence phenomena]. *Atti del XIV° Convegno nazionale di geotecnica, vol I.* Roma: Associazione geotecnica italiana,. 177-186.

García-Martín, J., J. Gómez-Gil, and E. Vázquez-Sánchez. 2011. Non-destructive techniques based on eddy current testing. *Sensors* 11(3): 2525-2565.

Gianneo, A., M. Carboni, M. Bellanova, and R. Felicetti. 2017. Study on the influence of defects on the strength of metallic historical tie-rods. Paper presented at the Arte17, 12th International Conference on non-destructive investigations and microanalysis for the diagnostics and conservation of cultural and environmental heritage (Art.17). Turin, November 22nd/24th.

Giussani, A. 2011. Relazione sulle misure eseguite per il controllo delle deformazioni del Duomo di Milano nei giorni 21, 23 e 28 Novembre 2011 [Report on deformation monitoring in the Cathedral of Milan on dates 21, 23 and 28 November 2011]. Politecnico di Milano (Lecco).

Heyman, J. 1995. *The stone skeleton : structural engineering of masonry architecture.* Cambridge: Cambridge University press.

IAEA, International Atomic Energy Agency. 2011. Training guidelines for Non-Destructive Testing techniques. Vienna.

ISO 3059: Non-destructive testing - Penetrant testing and magnetic particle testing - Viewing conditions.

L' Hèritier, M., P. Dillmann, S. Aumard, and P. Fluzin. 2013. Iron? Which iron? Methodologies for metallographic and slag inclusion studies applied to ferrous reinforcements from Auxerre Cathedral. In *The world of iron*. ed. J. Humphris and T. Rehren. Archetype Publications, 409-420.

Lagomarsino, S., and C. Calderini. 2005. The dynamical identification of the tensile force in ancient tie-rods. *Engineering Structures* 27(6): 846–856.

Maldague, X. P. 2001. *Theory and practice of infrared technology for nondestructive testing.* Wiley-Interscience.

Maldague, X., F. Galmiche, and A. Ziadi. 2002. Pulsed phase thermography reviewed. *dvances in pulsed phase thermography. Infrared physics & technology* 43(3): 175-181.

Mastrodicasa, S. 1974. *Dissesti statici delle strutture edilizie.* Milano: Hoepli.

Menzemer, C., E. Hilty, S. Morrison, R. Minor, and T. S. Srivatsan. 2016. Influence of post weld heat treatment on strength of three aluminum alloys used in light poles. *Metals* 6(3), 52.

Musso, and Copperi. 1877. *Particolari di costruzioni murali e finimenti di fabbricati: Parte 1.: Opere muratorie.* 3 riveduta ed accresciuta. G.B. Paravia.

Nicodemi, W. 2004. *The civilisation of iron: from prehistory to the third millennium.* Milano: Riva Group.

Percy, J. 1864. *Metallurgy: iron and steel.* London: John Murray.

Tullini, N., and F. Laudiero. 2008. Dynamic identification of beam axial loads using one flexural mode shape. *Journal of Sound and Vibration* 318(1): 131-147.

Tylecote, R.F. 1999. *A history of metallurgy.* London: The Metal Society.

Vasic, M. 2015. A multidisciplinary approach for the structural assessment of historical constructions with tie-rods. PhD diss. Politecnico di Milano.

Vecchiattini, R., C. Calderini, and P. Piccardo. 2015. Catene metalliche negli edifici storici in muratura. Primi risultati di una ricerca in corso. Edited by G. Biscontin and G. Driussi. *Scienza e beni culturali - Metalli in architettura. Conoscenza, Conservazione, Innovazione.* 63-73. Bressanone: Arcadia Ricerche.

Veneranda Fabbrica del Duomo. 1877. *Annali della Fabbrica del Duomo, dall'inizio al presente [Annals of Milan cathedral Fabbrica, from the beginning of the construction to the present]*. Milano: Ditta Gaetanto Brigola.

VV. AA.. 1987. *Stress intensity factor handbook.* Edited by Y. Murakami. Vol. I. Oxford: Pergamon Pres.

Wooh, S. C., and Y. Shi. 2001. Synthetic phase tuning of guided waves. *IEEE Transactions on utrasonics, ferroelectrics, and frquency control* 48(1): 209-223.

Yu, J. G., J. E. Lefebvre, Ch. Zhang, and F. E. Ratolojanahary. 2015. Dispersion curves of 2D rods with complex cross-sections: double orthogonal polynomial approach. *Meccanica* 50 (1): 109–117.

Zhongqing, S., and Y. Lin. 2009. *Identification of damage using lamb wave. From fundamentals to applications.* Vol. 48. Berlin: Springer Science & Business Media.

Figures captions

Table caption

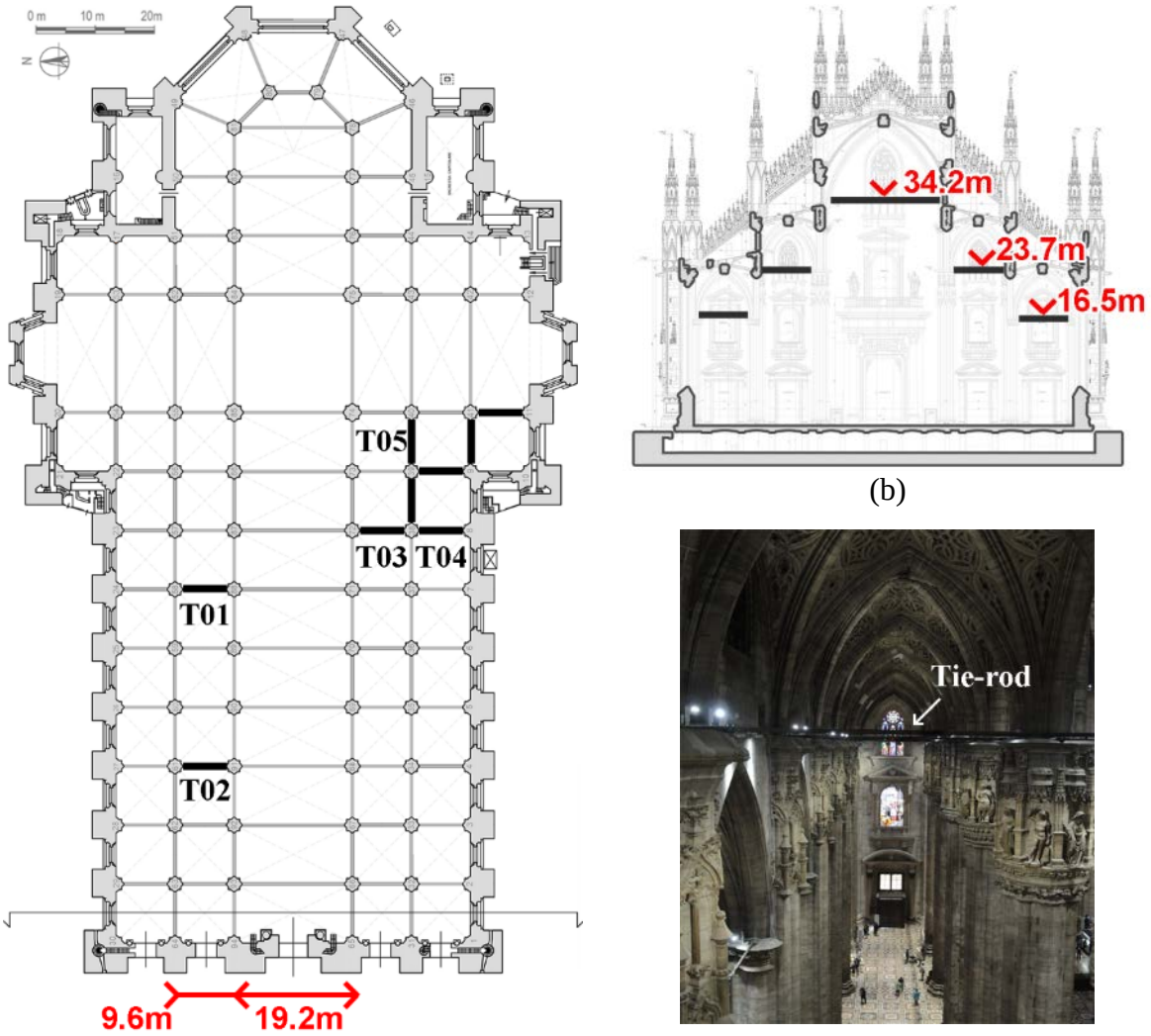

(a) (b) (c)

Figure 1. Milan Cathedral, (a) plan, (b) section, (c) internal view

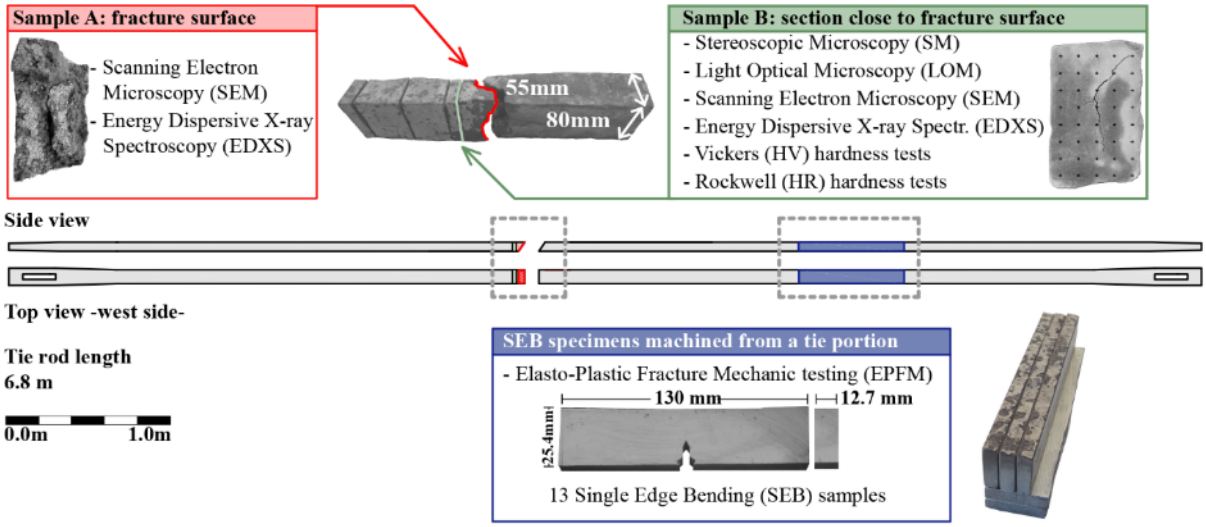

Figure 2: T01, location of samples used for material characterization

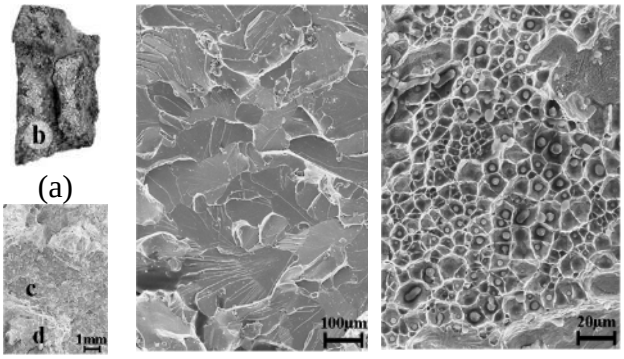

(a) (b) (c) (d)

Figure 3. SEM analyses on failure surface (sample A), (a) fracture surface, (b) general picture enlargement, (c) transgranular brittle failure area, (d) ductile failure area

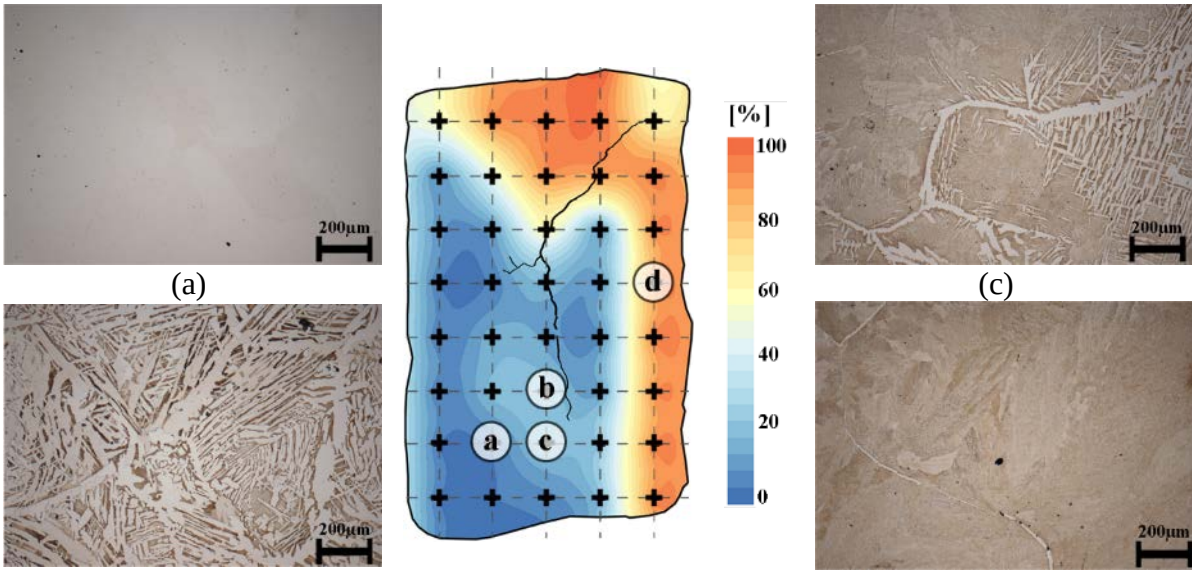

Figure 4. Pearlite distribution over the investigated cross-section (sample B) and typical micrographies at 100X, (a) pearlite 0%, (b) pearlite 20%, (c) pearlite 21%, (d) pearlite 97%

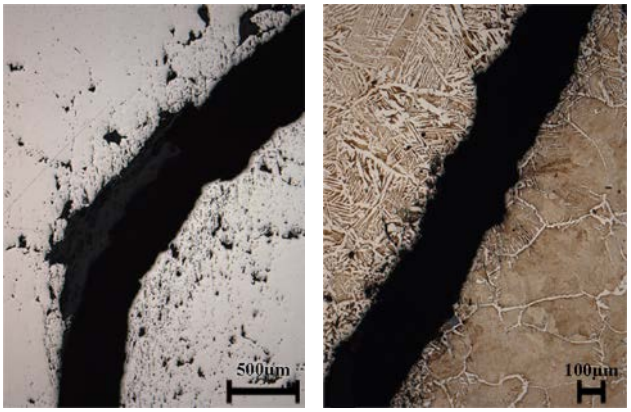

(a) (b)

Figure 5. LOM analyses close to crack on the investigated cross-section (sample B), (a) concentrated discontinuities, (b) sudden microstructure change

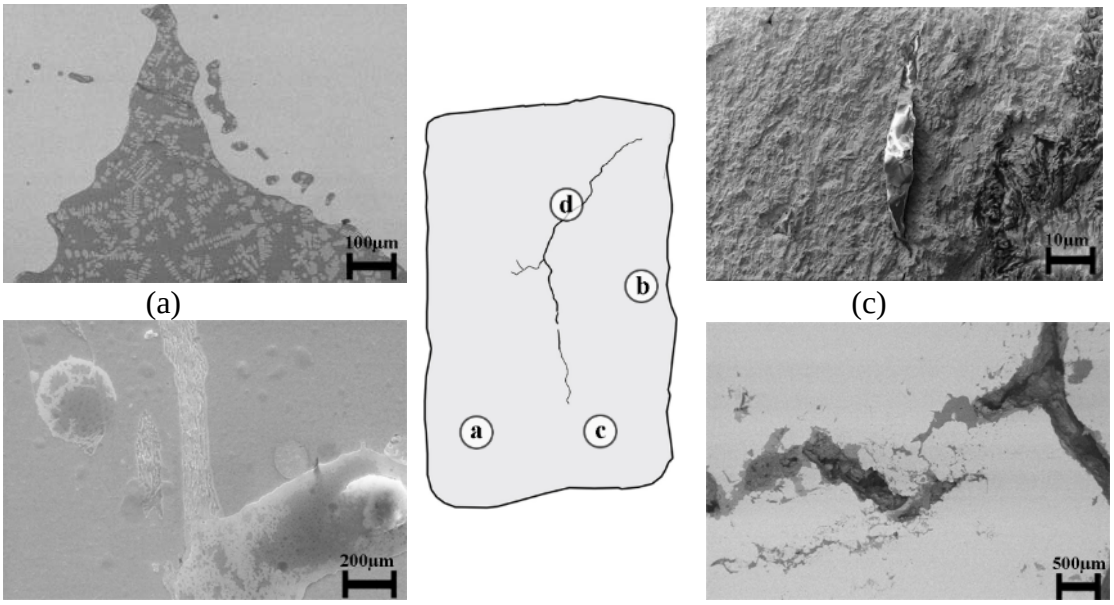

(a) (c)

(b) (d)

Figure 6. Micro discontinuities detected by SEM on the investigated cross-section (sample B) (a) iron-rich dendritic slag inclusion, (b) carbon-rich glassy inclusion, (c) spheroidal graphitic carbon, (d) iron-oxide inclusion inside crack

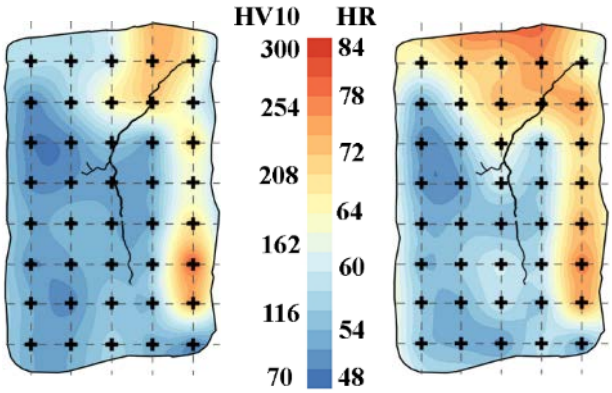

(a) (b)

Figure 7. Contour plots of hardness tests on the investigated cross-section (sample B)
(a) Vickers method, (b) Rockwell method

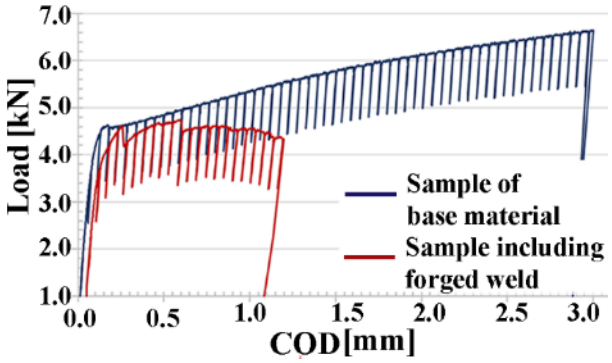

Figure 8. Load-displacement curves in Single Edge-Notched Bend (SEB) tests

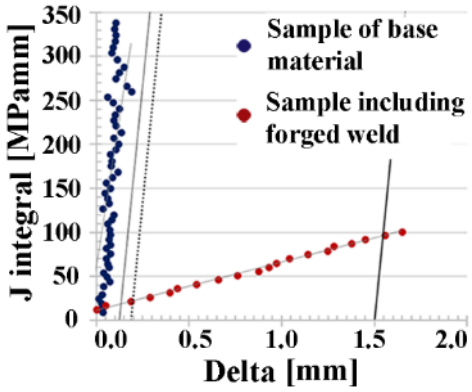

Figure 9. J intergral - resistance curves in Single Edge-Notched Bend (SEB) tests

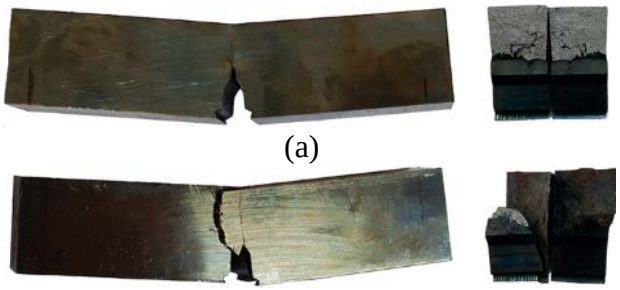

(a)

(b)

Figure 10. SEB specimens and their fracture surface after toughness test, (a) specimen of base material, (b) specimen including forged weld

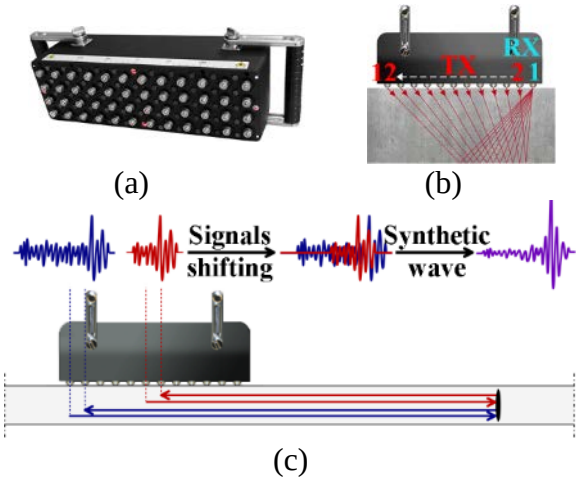

(a) (b)

(c)

Figure 11. Guided wave testing (a) MIRA A1040 tomograph, (b) data acquisition procedure, (c) processing procedure representation

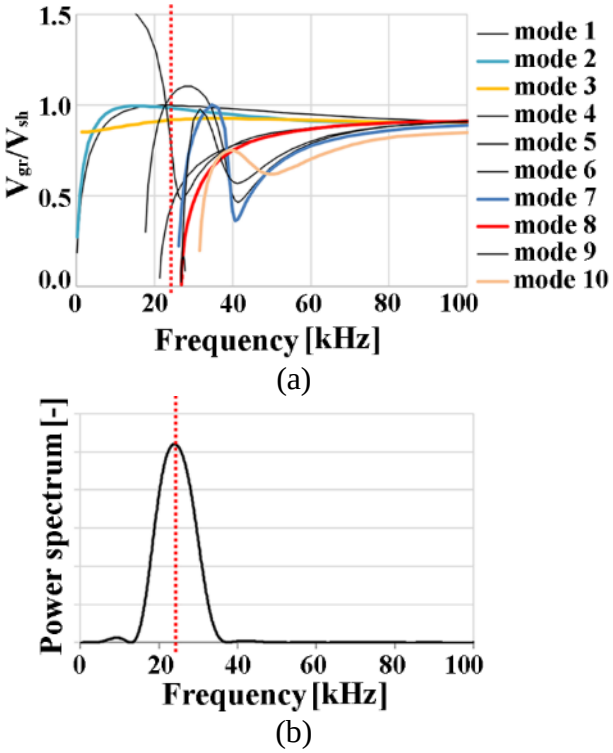

Figure 12. (a) Dispersion curves computed by the analytical polynomial approach, (b) power spectrum of the diagnostic wave

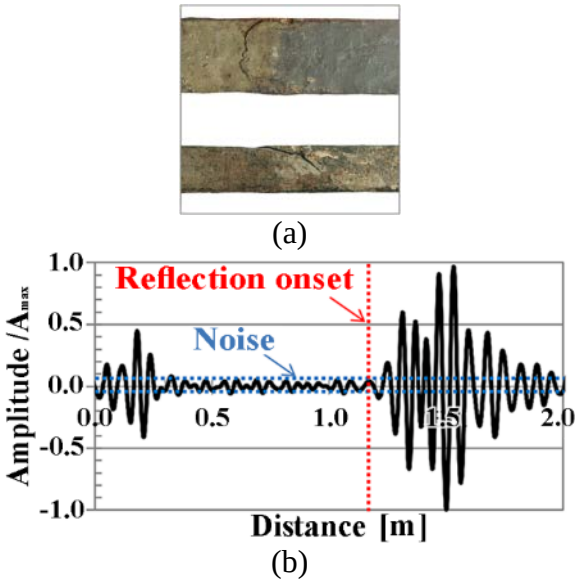

Figure 13. Laboratory experimental investigations on guided waves method (a) crack details, (b) wave amplitude-distance plot

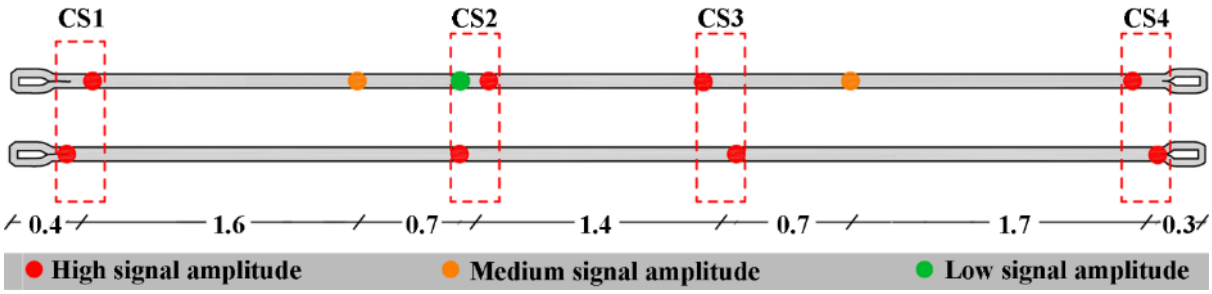

Figure 14. Discontinuities survey by using off-the-shelf spot probe

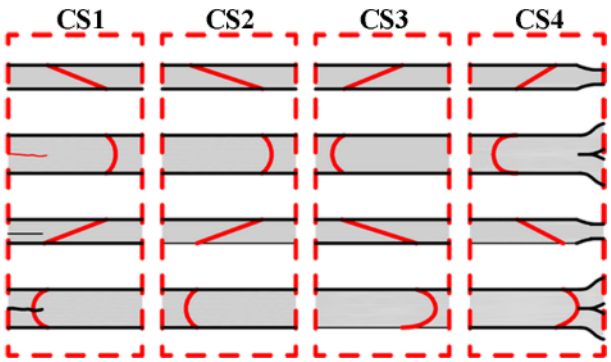

Figure 15. Discontinuities pattern survey by using magnetic particles inspection

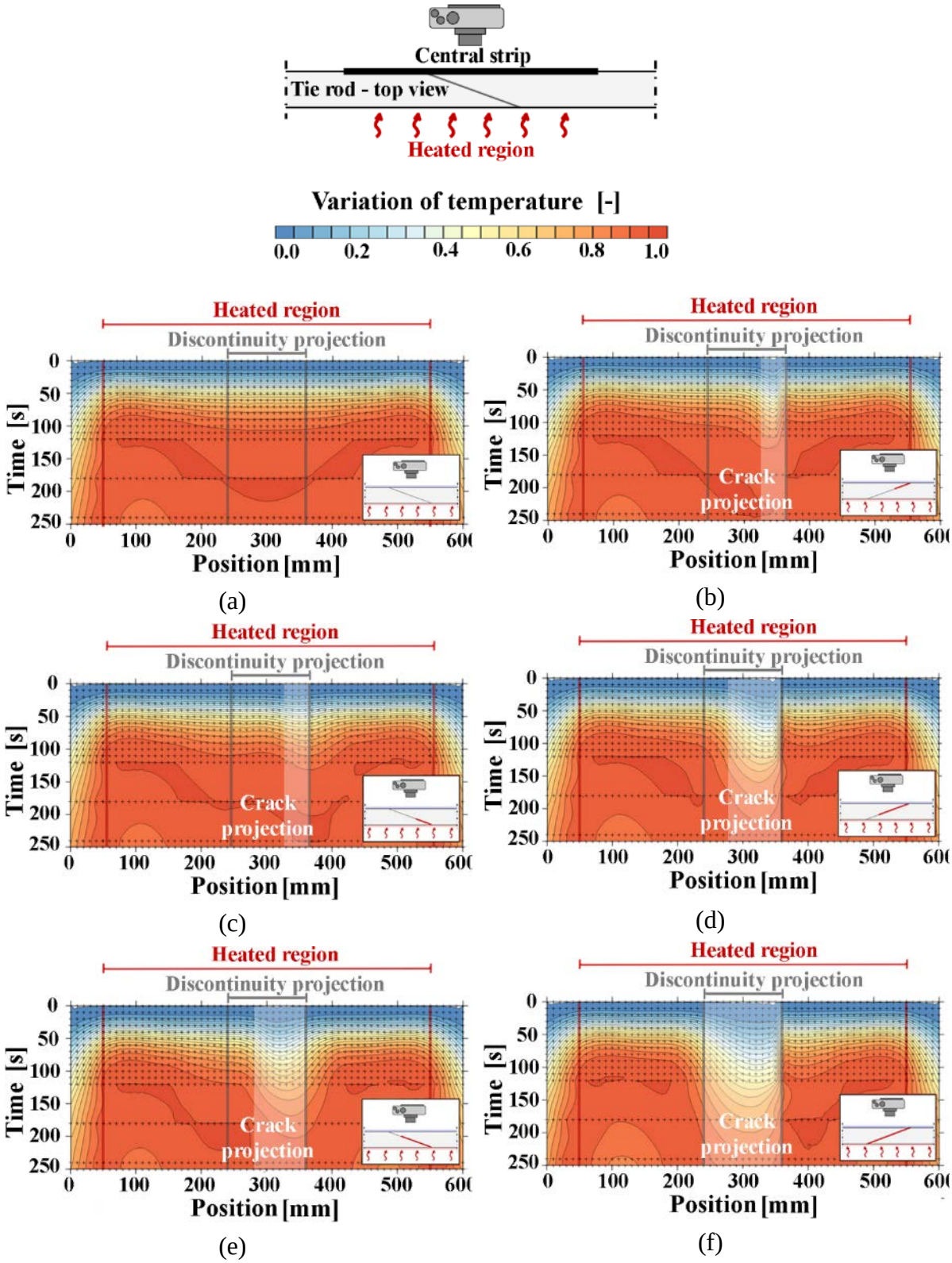

Figure 16. Numerical results of pulsed thermography, variation of temperature along a central strip, (a) discontinuity without defect (b) discontinuity with emerging crack involving one-third of the cross-section, (c) discontinuity with no-emerging crack involving one-third of the cross-section, (d) discontinuity with emerging crack involving two-third of the cross-section, (e) discontinuity with no-emerging crack involving two-third of the cross-section, (f) discontinuity with through-thickness crack

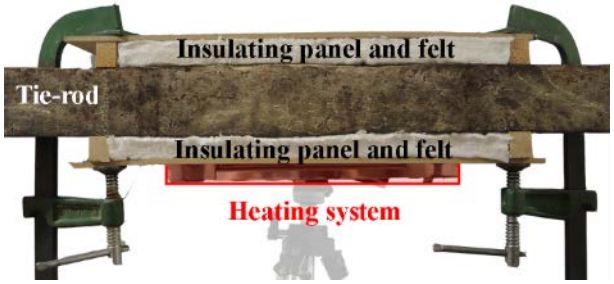

Figure 17. View from the observation side of the IR thermography showing the location of the thermal insulation to promote a planar thermal diffusion

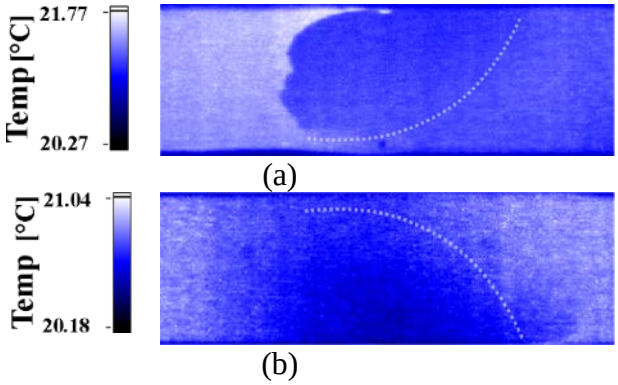

Figure 18. Experimental results of pulsed thermography, distribution of the maximum temperature T_{max} at the unexposed face ot the tie-rod (a) emerging crack, (b) non-emerging crack

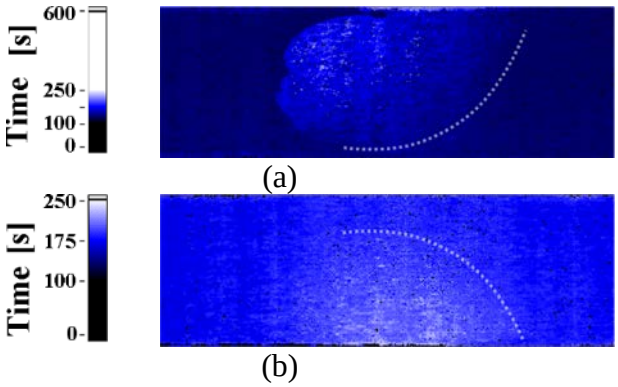

Figure 19. Experimental results of pulsed thermography, distribution of time t_{Tmax} corresponding to the maximum temperature T_{max} at the unexposed face ot the tie-rod (a) emerging crack, (b) non-emerging crack

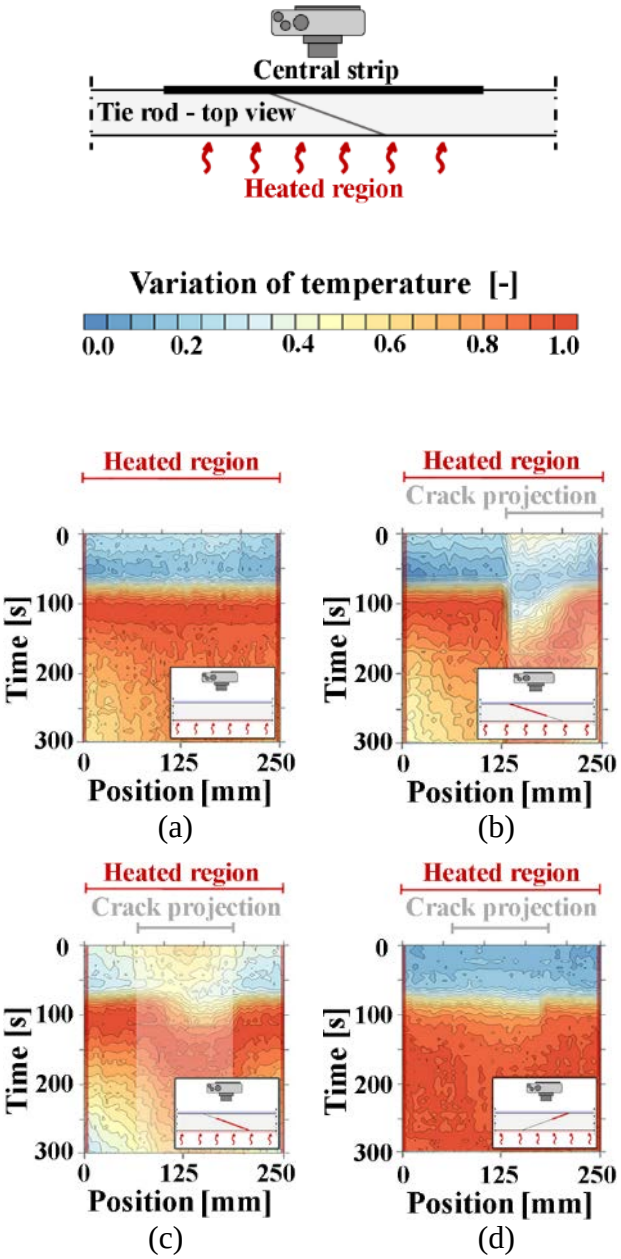

Figure 20. Experimental results of pulsed thermography, variation of temperature along a central strip, (a) region without discontinuity, (b) emerging macroscopic crack at forged weld, (c) minor non-emerging crack at the forged weld, (d) minor emerging crack at the forged weld detected by ET

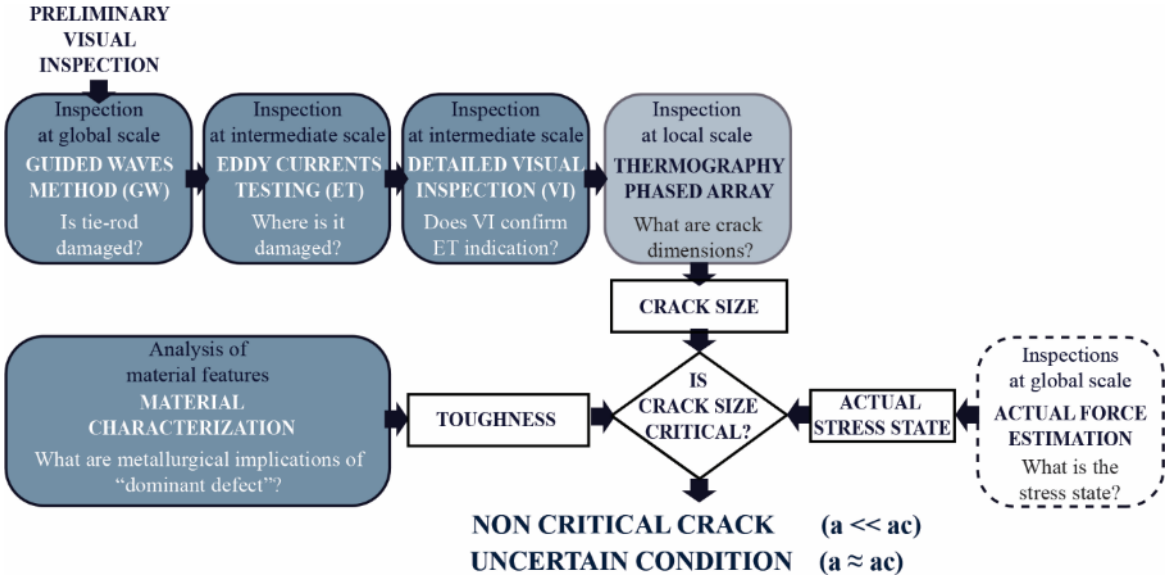

Figure 21. Flowchart of the proposed procedure

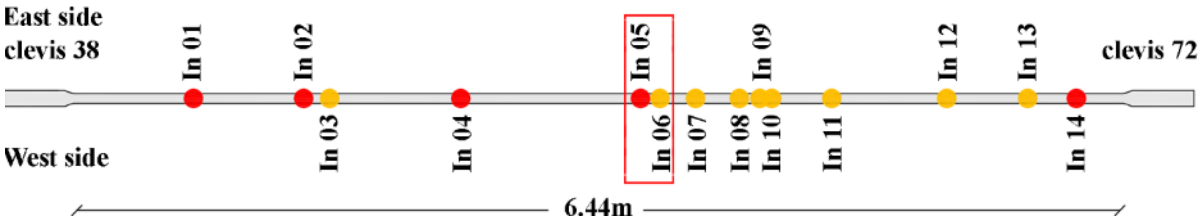

(a)

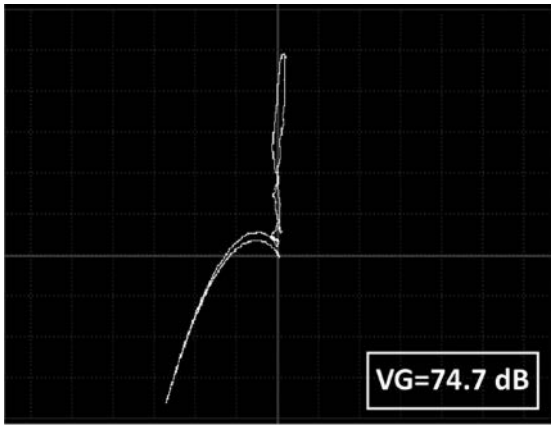

(b) (c) (d)

Figure 22. Results on tie-rod showing the most severe condition (a) detected ET indication, (b) impedance plane at In05, (c) detailed picture at In05, (d) crack highlighting

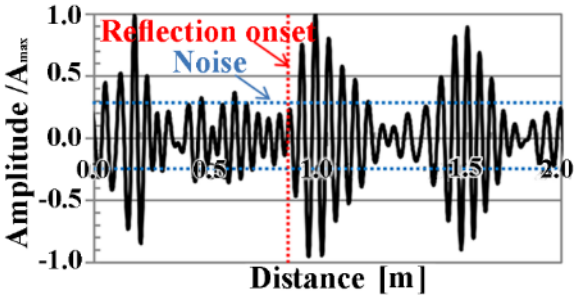

Figure 23. In-situ investigations on guided waves method (a) crack details, (b) wave amplitude-distance plot

	Guided Wave method via US tomograph GW	Low resolution Eddy current Testing ET	Pulsed Thermography PT
Scale	Global	Intermediate	Intermediate-local
Speed of test (data recording)	Fast	Medium	Slow
Representativeness	Depends on crack size	Good	Depends on crack location
Viability on site	High	High	Low
Ease of adaptation	Low	High	Low
Interpretation of results	Medium	Easy	Medium

Table 1. Comparison among the studied methods